

## Magnetic focusing and trapping of high-intensity laser-generated fast electrons at the rear of solid targets

J. R. Davies,\* A. R. Bell, and M. Tatarakis

Blackett Laboratory, Imperial College, London SW7 2BZ, United Kingdom

(Received 26 October 1998)

The transport of fast electrons generated by a 1 ps, 20 J,  $10^{19}$  W cm $^{-2}$ , 1  $\mu$ m wavelength laser pulse through 70–250  $\mu$ m thick deuterated polyethylene (CD2) targets is modeled with a Fokker-Planck hybrid code in  $r$ - $z$  geometry. Initially, electric field generation inhibits propagation, which then proceeds by the formation of a low resistivity channel due to Ohmic heating. The magnetic field generated at the edge of the channel leads to strong collimation. This is observed for a wide range of parameters. Reflection of electrons at the rear surface forms a magnetic field which focuses the incident electrons on to the rear surface and forces the reflected electrons outwards. This would lead to the formation of a small diameter plasma on the rear surface, as observed in experiments. The reflected electrons are confined to a cone by a self-generated magnetic field, enhancing energy deposition at the rear of the target. [S1063-651X(99)03705-8]

PACS number(s): 52.40.Nk, 52.50.Jm, 52.65.-y

### I. INTRODUCTION

High-intensity ( $>10^{18}$  W cm $^{-2}$ ), short-pulse lasers ( $<1$  ps) have opened up an area of research which has a number of applications [1]. An application which has received a lot of attention is the fast igniter inertial confinement fusion scheme [2]. In this it is proposed to use the fast electrons generated by a high-intensity, short-pulse laser to rapidly heat the core of a compressed deuterium tritium fuel pellet to ignition before it starts to decompress. A critical part of this scheme is the transport of the fast electrons from the lower density region where they are generated into the high-density core. Important information on fast electron generation and transport can be obtained from laser-solid experiments [3–6]. The interpretation of such experiments requires comparison with electron transport calculations. The transport of electron beams in solids and plasmas is also an active area of research in itself [7,8].

Here we model the transport of fast electrons generated by a 1 ps, 20 J,  $10^{19}$  W cm $^{-2}$ , 1  $\mu$ m wavelength laser pulse through 70–250  $\mu$ m thick plastic (CD2) targets, using the code described in [9] with the addition of magnetic diffusion. The parameters correspond to experiments on the VULCAN laser [3,5,6], which is typical of current high power lasers [1]. In these experiments plasma formation on the rear of 140 and 210  $\mu$ m thick CD2 targets was observed. The plasma was smaller in diameter and in line with the front plasma. This effect has also been observed in aluminum targets [10]. The aim here is to see if this phenomenon can be satisfactorily explained by magnetically collimated fast electron transport through the target, as suggested in [6], and if so what information can be inferred from it. An effect, due to electron reflection at the rear surface, of focusing of incident electrons and the concomitant forcing outwards of reflected electrons, is found. This provides the basis for developing

plasma formation on the rear of targets as a detailed diagnostic on fast electrons.

The code [9] uses a Fokker-Planck equation for the fast electrons. This is solved using stochastic differential equations, giving a particle Monte Carlo code. The background electrons are represented by  $\mathbf{E} = \eta \mathbf{j}_b$ , where  $\mathbf{j}_b$  is the background current density and  $\eta$  is the resistivity. The displacement current is neglected, giving

$$\mathbf{E} = -\eta \mathbf{j}_f + \frac{\eta}{\mu_0} \nabla \times \mathbf{B}, \quad (1)$$

$$\frac{\partial \mathbf{B}}{\partial t} = \nabla \times \eta \mathbf{j}_f - \nabla \times \frac{\eta}{\mu_0} \nabla \times \mathbf{B}, \quad (2)$$

where  $\mathbf{j}_f$  is the fast electron current density. We discuss these equations in [11]. We assume rotational symmetry giving fields  $E_r(r,z)$ ,  $E_z(r,z)$ , and  $B_\theta(r,z)$ . In [9] the final terms of Eqs. (1) and (2) were neglected. These have now been included, with implicit magnetic diffusion using an incomplete Choleski conjugate gradient (ICCG) routine [12]. As we are only concerned with fast electrons we now drop the term *fast*.

### II. CODE SET UP

For the electron generation we use a model laser intensity

$$I = I_p e^{-r^2/R^2} e^{-(t-t_p)^2/\tau^2} \quad (3)$$

with peak intensity ( $I_p$ )  $2 \times 10^{19}$  W cm $^{-2}$ , spot radius ( $R$ ) 6  $\mu$ m, pulse length ( $2\tau$ ) 1 ps, giving a pulse energy of  $\approx 20$  J, and pulse peak ( $t_p$ ) at 1 ps. The electrons are generated with an energy distribution going as  $e^{-K/kT}$ , where  $K$  is electron kinetic energy. The temperature ( $kT$ ) is calculated from the intensity [Eq. (3)] using the relation given in [3]

$$kT = 100 \left( \frac{I}{10^{17} \text{ W cm}^{-2}} \right)^{1/3} \text{ keV}, \quad (4)$$

\*Present address: GoLP, Instituto Superior Técnico, 1096 Lisboa Codex, Portugal.

which was determined from experiments on the VULCAN laser. The number of electrons generated per unit area per second is given by

$$F = \frac{f_{\text{abs}} I}{kT} \quad (5)$$

with absorption into electrons ( $f_{\text{abs}}$ ) 20%. The electrons were fired into the target down a cone of half angle  $15^\circ$ . Half angles of  $0^\circ$  and  $35^\circ$  were also used without significantly changing the main results.

Target thicknesses of 70, 100, 140, 170, 210, and 250  $\mu\text{m}$  were used. As electrons leave the rear surface and enter the vacuum they will set up an electrostatic field which will reflect them over a distance given by their Debye length [13,14]. As this is much less than the scale lengths of interest we specularly reflect the electrons at the rear surface, as at the front surface ( $z=0$ ) [9]. An alternative argument is that the current leaving the target still greatly exceeds the Alfvén-Lawson limit for propagation in vacuum [7]. Thus, to a good approximation, the current must be exactly cancelled by a reflected current. Two-dimensional particle-in-cell (PIC) modeling of electron emission into a vacuum from a plane conductor indicates that specular reflection is a good approximation [14]. Some electrons can escape the target, but this is strongly limited by space charge effects.

Collision coefficients were calculated in two ways; (1) the approach for a solid given in [9] and (2) the standard approach for a plasma for various degrees of ionization. The choice of coefficients did not significantly affect the overall results, the fields being dominant. The runs presented here use method 2 assuming  $\text{D}^+$  and  $\text{C}^{4+}$ . We chose these higher values to be certain that collisional effects are small and that the electron penetration is not overestimated.

The resistivity requires careful consideration. It is clear that the cold, insulator resistivity does not apply; using this value gives electric fields which would stop the electrons over a distance much less than their Debye length and completely ionize the atoms. Low-intensity experiments on the propagation of ionization fronts in insulating targets [15–17] show that the target will rapidly ionize at typical prepulse levels ( $\sim 10^{-6}$ ) of high-intensity lasers. Only  $\sim 0.6$  J is required to completely ionize every atom in a cylinder of CD2 with a radius of 12  $\mu\text{m}$  (twice the spot radius) and a length of 250  $\mu\text{m}$  (the thickest target considered). Thus, whether due to the prepulse, electrical break down due to fields generated by the fast electrons or collisional ionization by the fast electrons, the number density of free, background electrons will be similar to that in a metal. Using the expressions for electron mean free paths given in [18] we find that the mean interatomic spacing gives the greatest value up to a temperature of  $\sim 44$  eV, a regime known as resistivity saturation. At higher temperatures the classical formula gives the greater value. The electron de Broglie wavelength is less than the interatomic spacing for electrons with kinetic energy greater than 38 eV, so the classical formula should be valid. Resistivity saturation has been inferred in laser experiments with fused quartz targets [16], aluminum targets [19,20] and shocked liquid deuterium [21]. In all of these resistivities of  $\sim 2 \times 10^{-6}$   $\Omega\text{m}$  were obtained. This value approximately corresponds to a mean free path of the interatomic spacing, a

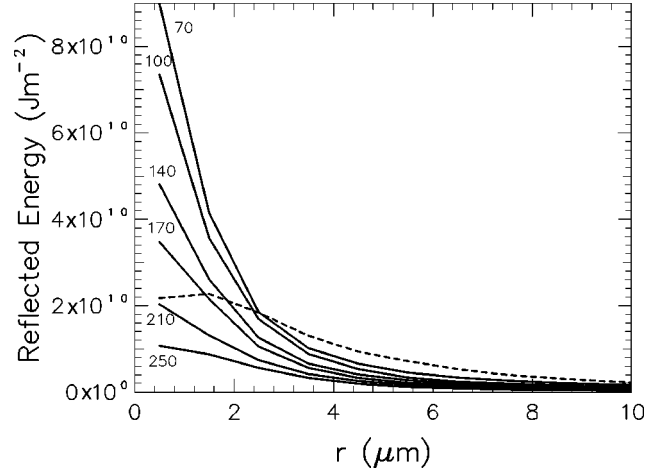


FIG. 1. Total energy per area reflected from the rear surface over 3 ps. Labels give target thickness. The radii at half maximum are, in order of increasing target thickness, 1.4, 1.5, 1.5, 1.8, 2.0 and 2.7  $\mu\text{m}$  and the total energy reflected within a radius of 3  $\mu\text{m}$  is 0.96, 0.83, 0.60, 0.48, 0.30, and 0.20 J. The dotted line is for that crossing  $z = 70$   $\mu\text{m}$  in a thicker target.

conduction electron number density of  $\sim 10^{29}$   $\text{m}^{-3}$  (solid density) and a temperature of some eV. So we chose a function which starts at such a saturated value and tends to the classical result at high temperatures

$$\eta = \frac{1}{1/\eta_0 + 1/\eta_{\text{Spitzer}}} \quad (6)$$

with  $\eta_0 = 2.3 \times 10^{-6}$   $\Omega\text{m}$ ,  $\eta_{\text{Spitzer}} = 10^{-4} Z \ln \Lambda (kT_b)^{-3/2}$   $\Omega\text{m}$  and  $Z \ln \Lambda = 8$ , where  $kT_b$  is the temperature increase of the background in eV. The conduction-electron number density used in calculating  $\eta_0$  corresponds to roughly one free electron per atom. Significantly higher values of  $\eta_0$  were found to give electric fields sufficient to cause field ionization, which would almost instantly lower the resistivity.

For the specific-heat capacity (SHC) we use the value for an ideal electron gas assuming  $\text{D}^+$  and  $\text{C}^{4+}$ . Although the solid's SHC is much lower than this it would be increased by energy loss to ionization.

The computational parameters were  $\Delta r = 0.5$   $\mu\text{m}$ ,  $\Delta z = 0.5$  or 1  $\mu\text{m}$ ,  $\Delta t = 1.67$  fs, grid radius 50  $\mu\text{m}$ , 500 computational particles generated per time step, and run time 3 or 4 ps. The maximum number of particles on the grid was  $\approx 5 \times 10^5$ . The same detailed checks on the consistency of the results with the approximations used were carried out as described in [9].

### III. RESULTS

For plasma generation on the rear surface the most fundamental result is the radial distribution of electron energy striking the rear surface (Fig. 1). This gives the maximum energy available to form a plasma in a given area. In each case this is sharply peaked within a radius approximately half that of the laser spot. With the field generation turned off, i.e., only collisions, the results are not comparable. A fraction of an electron's energy would be lost on reflection to driving the expansion of any plasma formed, but without

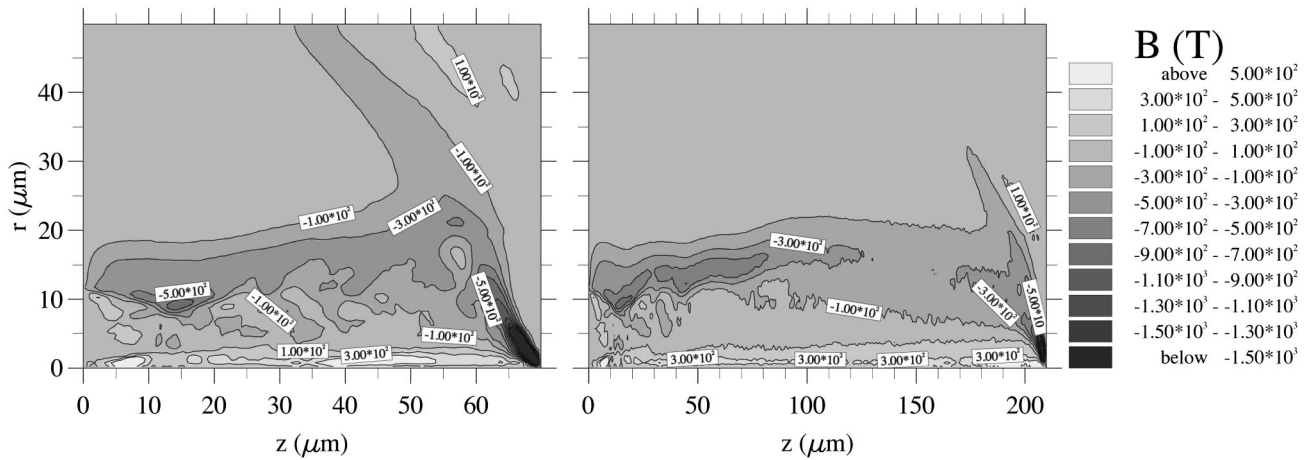


FIG. 2. Magnetic field (T) at 3 ps for the 70 and 210  $\mu\text{m}$  thick targets. Similar patterns are observed for the other thicknesses.

further calculation it is not clear what this would be. So we can only state that sufficient energy is delivered to the rear surface, within a radius less than that of the laser spot, to generate a plasma. We will return to the generation of plasma on the rear of the target later, we will now consider the electron transport which leads to such a pattern.

Initially the electric field prevents electron propagation [22]. This leads to strong heating of the background, lowering the resistivity and hence the electric field, allowing the electrons to propagate. Thus electron propagation proceeds by the formation of a low resistivity channel. This is more efficient on the axis, where the current density is higher, as the effect of the lowering of the resistivity due to Ohmic heating eventually outweighs the increase in electric field with current density [Eq. (1)]. Regions which initially have a higher current density, and hence higher electric field, end up having a lower electric field. This effect is basically Haines' electrothermal instability [23]. The radial variation in the inhibiting electric field [the  $-\eta\partial j_z/\partial r$  term in Eq. (2)] rapidly generates a negative magnetic field which acts to pinch the electron flow. However, the subsequent fall in the electric field due to the Ohmic heating lowers the magnetic field [the  $-(\nabla\eta)_r j_z$  term in Eq. (2)] and eventually generates a positive magnetic field just off axis (Fig. 2). This effect limits the pinching of the electron beam by the magnetic field. The resultant off-axis magnetic field null gives a second point onto which the electron flow is pinched. However, the magnetic field does not become high enough to produce two distinct filaments. The formation of a low resistivity channel, with low fields within it and a collimating magnetic field at the edge, leads to an electron beam propagating straight through the target, with a diameter which remains comparable to that of the source.

The main factors affecting the energy reaching the rear surface are (1) the resistivity, which determines the electric field [Eq. (1)], and (2) the SHC, which determines the energy needed to form the low resistivity channel. We now consider the effect of varying the resistivity and the SHC in the 210  $\mu\text{m}$  run. Reducing the resistivity by a factor of 10 did not affect the electron collimation. The peak in energy per area striking the rear surface moved 1–2  $\mu\text{m}$  off axis and fell by a factor of 0.7, at larger radii it was slightly increased. The total energy striking the rear surface increased by a fac-

tor of 2.2. Increasing the resistivity by a factor of 10 prevented the low resistivity, magnetized channel from reaching the rear surface. Thus there was no sharp peak in the energy per area striking the rear surface, the peak value was a factor of  $10^3$  lower. The total energy striking the rear surface was reduced by a factor of 0.21. This result does not agree with experiments, reinforcing our argument that such a high resistivity is unphysical. Increasing or decreasing the SHC by a factor of 2 did not affect the general features of the electron transport; the total energy striking the rear surface changed by factors of 0.67 and 1.4, respectively.

As can be seen from Figs. 1 and 2 the electron flow is pinched inwards towards the rear of a target by a strong magnetic field. There is clearly a focusing of the electrons onto the rear surface, due to the presence of the rear surface. This is caused by reflected electrons which are moving radially outwards. The majority of the electrons striking the rear surface are moving outwards and the magnetic field at the edge of the beam, which collimates the incident electrons, turns reflected electrons outwards. The magnetic field then generated by these reflected electrons increases this magnetic field, giving an instability. A simple physical picture of this effect is that the incident and reflected electrons form oppositely directed currents which repel one another. This pinches in the incident electrons and pushes out the reflected electrons. The magnetic field generated by reflected electrons moving radially outwards (Fig. 2) confines them to a cone. This enhances energy deposition behind the rear surface (Fig. 3). This gives an additional effect to be considered in the interpretation of layered target  $K\alpha$  emission experiments [9,11]. Reducing the resistivity by a factor of 10 gave a lower magnetic field which did not give such a pronounced cone. If the electrons are diffusely reflected the cone of reflected electrons is also less pronounced and energy deposition just behind the rear surface is slightly reduced. However, the focusing still occurs, the curves in Fig. 1 are only marginally broadened.

The heating of the targets (Fig. 4) at the rear surface would lead to the formation of a small diameter plasma, without any further heating from reflected electrons. The cone of reflected electrons is also clearly revealed in these plots. The electric field generated as the electrons are reflected can be estimated [14] to be

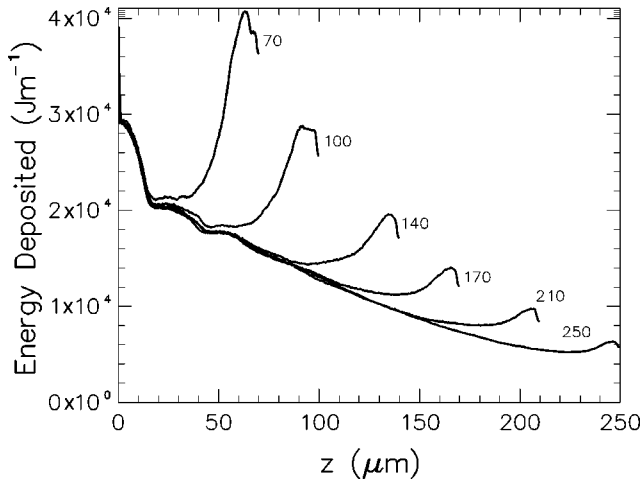


FIG. 3. Energy deposited per meter over 3 ps as a function of distance into the target ( $z$ ). Labels give target thickness. The total energy deposited over 3 ps is, in order of increasing target thickness, 2.2, 2.4, 2.7, 2.8, 3, and 3.1 J. The sharp peak at  $z=0$  is due to the low-energy electrons in the distribution used.

$$E \approx \frac{kT_r}{e\lambda_D} \sim 1.3 \times 10^{-4} (n_r)^{1/2} (kT_r)^{1/2} \text{ V m}^{-1}, \quad (7)$$

where  $kT_r$  is the temperature in eV,  $\lambda_D$  the Debye length and  $n_r$  the number density of the electrons reflected. This can be estimated from Fig. 1, the mean electron speed ( $\sim 0.8c$ ) and the time for which electrons have been arriving. This gives, time averaged, peak electric fields of  $\sim 10^{12} \text{ V m}^{-1}$  for each target thickness. (There is a factor of 2.4 difference between the 70 and 250  $\mu\text{m}$  targets.) Such an electric field would ionize the rear surface and accelerate ions outwards. Thus there will be additional heating at the rear surface from electrons reflected near the axis.

When the resistivity was increased by a factor of 10 the heating of the target showed quite a different pattern from Fig. 4. There was a radial spread of approximately 40  $\mu\text{m}$  in the region  $z \approx 10\text{--}20 \mu\text{m}$ . This is a result of radial diffusion of the background current [the last term in Eq. (1)]. The Ohmic heating it causes leads to lateral electron transport in the same manner as the ‘‘channeling’’ discussed above. Al-

though this resistivity is unrealistic, as the scale length of the diffusion scales as  $\sqrt{\eta\tau}$ , where  $\tau$  is time, this process could occur for longer pulses. This and the formation of a cone of reflected electrons provide additional mechanisms which could explain lateral electron transport to those discussed in [9] and [14].

#### IV. CONCLUSIONS

We find that magnetic-field collimation of electrons is a feature which is to be expected in high intensity laser-solid experiments, being present in simulations for a wide range of parameters. A lesser degree of collimation was present in runs for aluminum at  $10^{18} \text{ W cm}^{-2}$  [9]. Collimation is enhanced by the formation of a low resistivity channel, which also prevents the beam being pinched inwards by the magnetic field.

Reflection of electrons at the rear surface forms a magnetic field which focuses electrons onto the rear surface. This focusing will occur whenever a strong current of charged particles is incident on a reflective, or partially reflective, boundary. For the targets considered the flux of electrons at the rear surface is easily sufficient to ionize it and generate a small diameter plasma. This explains experimental observations [5,6]. It gives a diagnostic on fast electron generation and transport, by comparing measurements of the plasma formation with calculations such as those given here. The results given here show that the diameter of the rear plasma is not a direct indicator of the collimation within the target. In this case the beam within the target has approximately twice the diameter of the rear plasma (Fig. 1).

Electron collimation would have important implications for the fast igniter scheme [2] as it would increase the energy reaching the core. It would also make the alignment of the ignition pulse more critical as the electrons could miss the core altogether. The target densities the electrons must reach in the fast igniter scheme are much higher than the solid targets considered here. Higher densities give a lower saturated resistivity, higher heat capacity and higher collision coefficients. The wide range of parameters covered here indicate that magnetic-field collimation will be important in fast igniter conditions, but further calculations are required.

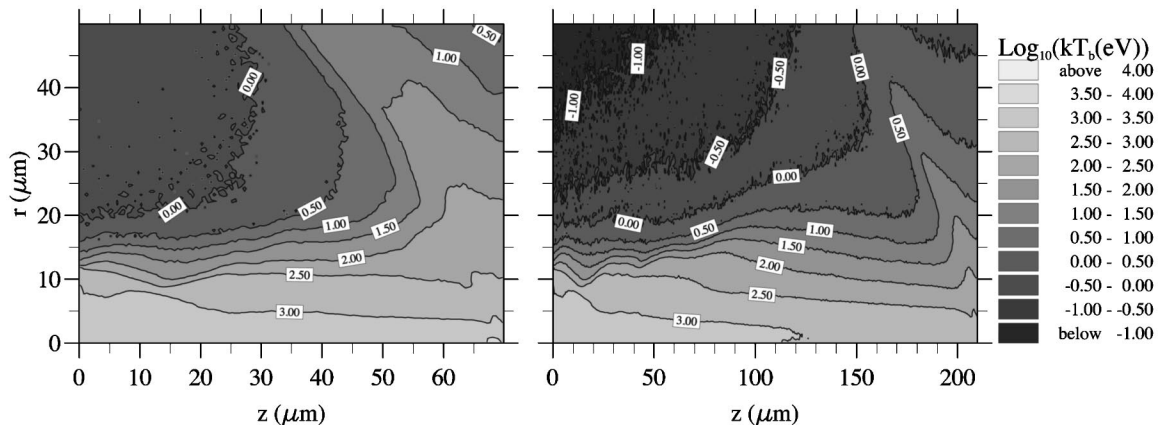


FIG. 4.  $\log_{10}$  of the temperature increase (eV) over 3 ps for the 70 and 210  $\mu\text{m}$  thick targets. Similar patterns are observed for the other thicknesses. The peak temperatures at the rear surface are, in order of increasing target thickness, 3.6, 2.2, 1.6, 0.94, 0.78, and 0.44 keV. For the 70 and 100  $\mu\text{m}$  targets the peak is on axis, for the others it is 0.5–1  $\mu\text{m}$  off axis.

Kink (or hosing) instabilities [7,24] are not included in the code, because of the cylindrical geometry used. They were not observed in the experiments with plastic targets, where the rear plasma was always in line with that on the front [5,6]. The formation of the low resistivity channel and consequent reduction of the magnetic field which drives these instabilities will act to prevent them. Motion of the beam into the high resistivity region surrounding it would also be opposed by a strong electric field. In the models used in [7] and [24], which show such instabilities, the resistivity is fixed. Small deviations have been observed in aluminum targets, but only at lower intensities ( $\sim 10^{17}$  W cm $^{-2}$ ) [10] (this will be the subject of a future publication). This is consistent with this explanation as the resistivity of aluminum increases up to a temperature of  $\sim 50$  eV [19], so a low resistivity channel will only form if it is heated to well above this temperature. This would not occur at low intensities. Thus it appears that the lowering of the resistivity by Ohmic heating, which limits the pinching of the electron beam, could also prevent

kink instabilities. The stability of these beams to the kink instability requires further study.

The possible development of microinstabilities [7,25] in the plasma formed in the target, increasing the resistivity, is not included. This could counteract the formation of a low resistivity channel and increase the energy loss. However, we have seen that a significant increase in the resistivity leads to results which contradict experiments.

The measurement of magnetic fields in solid targets is extremely difficult. A beam of electrons fired through the target could be used as a diagnostic.

#### ACKNOWLEDGMENTS

We acknowledge useful discussions with M. G. Haines, A. E. Dangor, and P. A. Norreys. This work was supported by U.K. EPSRC Grant No. GR/K19198 and by the European TMR Programme under Contract No. ERBFMBICT983502.

- 
- [1] P. Gibbon and E. Förster, *Plasma Phys. Controlled Fusion* **38**, 769 (1996).
- [2] M. Tabak, J. M. Hammer, M. E. Glinsky, W. L. Kruer, S. C. Wilks, and J. Woodworth, *Phys. Plasmas* **1**, 1626 (1994).
- [3] F. N. Beg, A. R. Bell, A. E. Dangor, C. N. Danson, A. P. Fews, M. E. Glinsky, B. A. Hammel, P. Lee, P. A. Norreys, and M. Tatarakis, *Phys. Plasmas* **4**, 447 (1996).
- [4] M. H. Key, M. D. Cable, T. E. Cowan, K. G. Estabrook, B. A. Hammel, S. P. Hatchet, E. A. Henry, D. E. Hinkel, J. D. Kilkenny, J. A. Koch, W. L. Kruer, A. B. Langdon, B. F. Lasinski, R. W. Lee, B. J. MacGowan, A. MacKinnon, J. D. Moody, M. J. Moran, A. A. Offenberger, D. M. Pennington, M. D. Perry, T. J. Phillips, T. C. Sangster, M. S. Singh, M. A. Stoyer, M. Tabak, G. L. Tietbohl, M. Tsukamoto, K. Wharton, and S. C. Wilks, *Phys. Plasmas* **5**, 1966 (1998).
- [5] M. Tatarakis, Ph.D. thesis, University of London, 1996 (unpublished).
- [6] M. Tatarakis, J. R. Davies, P. Lee, P. A. Norreys, N. G. Kasapakis, F. N. Beg, A. R. Bell, M. G. Haines, and A. E. Dangor, *Phys. Rev. Lett.* **81**, 999 (1998).
- [7] R. B. Miller, *Intense Charged Particle Beams* (Plenum, New York, 1982).
- [8] M. V. Nezlin, *Physics of Intense Beams in Plasmas* (IOP, London, 1993).
- [9] J. R. Davies, A. R. Bell, M. G. Haines, and S. M. Guerin, *Phys. Rev. E* **56**, 7193 (1997).
- [10] A. E. Dangor (private communication).
- [11] A. R. Bell, J. R. Davies, and S. M. Guerin, *Phys. Rev. E* **58**, 2471 (1998).
- [12] D. S. Kershaw, *J. Comput. Phys.* **26**, 43 (1978).
- [13] H. Hora, *Physics of Laser Driven Plasmas* (Wiley, New York, 1981).
- [14] J. R. Davies, Ph.D. thesis, University of London, 1997.
- [15] F. Amiranoff, R. Fedosejevs, R. F. Scmalz, R. Sigel, and Yung-lu Teng, *Phys. Rev. A* **32**, 3535 (1985).
- [16] B. T. Vu, O. L. Landen, and A. Szoke, *Phys. Plasmas* **2**, 476 (1995).
- [17] T. Ditmire, E. T. Gumbrell, R. A. Smith, L. Mountford, and M. H. R. Hutchinson, *Phys. Rev. Lett.* **77**, 498 (1996).
- [18] Y. T. Lee and R. M. More, *Phys. Fluids* **27**, 1273 (1984).
- [19] H. M. Milchberg, R. R. Freeman, S. C. Davey, and R. M. More, *Phys. Rev. Lett.* **61**, 2364 (1988).
- [20] A. Saemann and K. Eidmann, in *Superstrong Fields in Plasmas*, editors M. Lontano, G. Mourou, F. Pegoraro, and E. Siondi, AIP Conf. Proc. No. **426** (AIP, New York, 1998), p. 270.
- [21] P. M. Celliers, presentation at XXV ECLIM, Formia, Italy, 1998.
- [22] A. R. Bell, J. R. Davies, S. Guerin, and H. Ruhl, *Plasma Phys. Controlled Fusion* **39**, 653 (1997).
- [23] M. G. Haines, *Phys. Rev. Lett.* **47**, 917 (1981); M. G. Haines and F. Marsh, *J. Plasma Phys.* **27**, 427 (1982).
- [24] T. Yabe, K. Mima, T. Sugiyama, and K. Yoshikawa, *Phys. Rev. Lett.* **48**, 242 (1982).
- [25] T. Yabe, K. Mima, K. Yoshikawa, H. Takabe, and M. Hamano, *Nucl. Fusion* **21**, 803 (1981).